Journal of
Manufacturing and Materials Processing

MDPI

Article

Laser Beam Welding under Vacuum of Hot-Dip Galvanized Constructional Steel

Christian Frey [1,*], Ole Stocks [1], Simon Olschok [1,*], Ronny Kühne [2], Markus Feldmann [2] and Uwe Reisgen [1]

[1] Welding and Joining Institute, RWTH Aachen University, Pontstr. 49, 52062 Aachen, Germany
[2] Institute of Steel Construction, RWTH Aachen University, Mies-van-der-Rohe-Str. 1, 52074 Aachen, Germany
* Correspondence: frey@isf.rwth-aachen.de (C.F.); olschok@isf.rwth-aachen.de (S.O.)

Abstract: Hot-dip galvanized components offer a great potential for corrosion protection of up to 100 years, while laser beam welding in vacuum (LaVa) has the advantage of high penetration depths Combined, this process chain can be economically used in steel construction of bridges, wind turbines, or other steel constructions. Therefore, investigations of butt joint welding of galvanized 20 mm thick S355M steel plates using LaVa were carried out. The butt joints were prepared under different cutting edges such as flame-cut, sawn, and milled edges, and they were studied with and without the zinc layer in the joint gap. For this purpose, the laser parameters such as the beam power, welding speed, focus position, and working pressure all varied, as did the oscillation parameters. The welds performed using an infinity oscillation with an amplitude of 5 mm represented a pore-free weld up to a zinc layer thickness of 400 µm in the joint gap. The seam undercut increased with increasing the zinc layer thickness in the joint gap, which can be explained by the evaporating zinc and consequently the missing material, since no filler material was used. The joint welds with zinc only on the sheet surface achieved a sufficient weld quality without pores.

Keywords: laser beam welding; vacuum; hot-dip galvanizing; S355; LaVa

Citation: Frey, C.; Stocks, O.; Olschok, S.; Kühne, R.; Feldmann, M.; Reisgen, U. Laser Beam Welding under Vacuum of Hot-Dip Galvanized Constructional Steel. *J. Manuf. Mater. Process.* **2024**, *8*, 17. https://doi.org/10.3390/jmmp8010017

Academic Editor: Ivan Galvão

Received: 27 December 2023
Revised: 15 January 2024
Accepted: 18 January 2024
Published: 22 January 2024

1. Introduction

Laser beam welding under vacuum (LaVa) offers the advantage of large welding depths [1], while hot-dip galvanized components offer significant potential for corrosion protection of up to 100 years [2]. Combining these processes in the steel construction industry—especially for bridges and wind turbines—can increase productivity and sustainability. The fabrication of large structural buildings is constrained by the complicated and expensive manufacturing process of the steel components [1]. Moreover, hot-dip galvanizing of large structures is problematic due to the limited zinc pool size and temperature gradients over the size of the component, which can lead to constraints and uneven expansions and consequently to crack formation, especially liquid metal embrittlement (LME) [3]. From a manufacturing and economic point of view, it is more cost effective to galvanize smaller semi-finished products before welding them together. These smaller semi-finished products reduce the complexity, the size of liquid zinc pool, as well as the heavy transporter size. In steel bridge constructions, the joining of hot-dip galvanized components is carried out by protecting the areas of the future joints from zinc layer formation during the galvanizing process with masking paint [4]. The masking varnish will be removed, and the joining process is carried out on the locally ungalvanized joining partners. Afterwards, the joint itself and the surrounding ungalvanized area are again protected against corrosion by spray metallization [1]. Often, these connections are welded with multilayers technology using conventional arc processes. An alternative method can be laser beam welding in a vacuum (LaVa), which enables welding depths of up to 110 mm in butt joint connection while generating a small heat-affecting zone [5]. The high focused energy input of LaVa can evaporate the zinc from the joining gap while the welding process takes place. In

addition to typical stationary processes, the use of a mobile laser welding system (MoVak) is conceivable, which already generates welding depths of up to 40 mm [6]. However, the fast-evaporating zinc coating leads to process instabilities and results in welding defects. To overcome this process limit for LaVa, this paper examines the influence of beam oscillation geometry on joining hot-dip galvanized thick metal sheets.

2. State of Art

2.1. Hot-Dip Galvanizing

Hot-dip galvanizing is a non-detachable corrosion protection process in which a cathodic protection effect occurs because of the element zinc, which is less noble than iron. The zinc becomes a galvanic anode and minor damage to the zinc layer does not automatically lead to a loss of corrosion protection [7]. In this process, the pickled and fluxed steel immerses in a liquid zinc melt at temperatures of approx. 450 °C. Thus, zinc deposits directly on the surface and creates differently concentrated hard and brittle phases out of iron–zinc alloys. On top of the intermetallic phases, a phase of pure zinc enriches the surface. The zinc layer thickness mainly depends on the silicon content of the steel. Those phases form through diffusion of the liquid zinc with the surface and depend on the melting temperature, the time in the zinc bath, and the steel composition. From a metallographic point of view, the iron–zinc layer consists of a heterogeneous structure. The different phases are characterized by different degrees of hardness and, due to their adhesion, have a high resistance to the removal of the layers or other mechanical loads [8]. Seen from the sample, the Γ-, δ- and ζ-phase form the iron–zinc alloy layer, which is completed by the η-phase, which is a pure zinc layer. The alloying elements silicon and phosphorus have a significant influence on the formation of the zinc coating. The proportion of the ζ-phase in particular increases with a higher silicon content [9]. For this reason, structural steels to be galvanized are divided into four different areas, the low-silicon, Sandelin, Sebisty, and high-silicon areas, which are differentiated according to their respective silicon and phosphorus content. When galvanizing steel in the Sebisty range, much lower zinc layer thicknesses are to be expected than in the Sandelin or high silicon range. In addition to the alloying elements, the immersion time also influences the thickness of the zinc coating. This increases with increasing the immersion or dwell time in the zinc bath [3]. According to the German Standard DIN EN 14713-2 [10], the various thermal cutting processes (plasma cutting, oxy-fuel cutting, laser cutting) also have an influence on the zinc layer thickness, as the steel composition and microstructure change in the area of the cut surface. The oxidation of silicon-to-silicon oxide results in silicon deactivation, which causes the steel to be in the low silicon range locally. This reduces the thickness of the zinc coating. Therefore, the resulting surfaces should be ground down and sharp edges removed when using the thermal separation process in order to ensure a reliable coating thickness. In the welding process, the cut edge preparation essentially determines the joint gap width [11], which can lead to deeper penetration depth or seam collapse [12]. In addition, impurities such as thick scale layers on the cut edge can lead to process instability in the form of strong welding spatters. In the galvanizing process, the immersion process is the most critical factor, as it involves uneven heating and therefore prevents constant thermal expansion in the component. In addition, during the galvanizing process of steel structures, there are various mechanical influences due to different conditions. These conditions include stationary and transient conditions during immersion or while the material is dwelling in the molten zinc. These conditions, in turn, have an influence on the temperature, the strain development, and the ductility development of the components [3]. As a result, they can lead to cracking during the hot-dip galvanizing process and consequently to liquid metal-induced stress corrosion cracking [13]. The study shows a wide variety of liquid metal-induced stress corrosion cracking applications, such as a crack in a bottom chord of a floor beam.

2.2. Laser Welding

The first study for laser beam welding in vacuum attempts to suppress the plasma flare above the weld, which is harmful for welding with the CO_2 laser and can scarcely be avoided under ambient pressure [14]. Thereby the results established a strong correlation between the working pressure and the achieved welding depth in deep penetration welding. With the shorter wavelength of Nd:YAG solid-state lasers, the plasma flare is almost suppressed and further investigations focused largely on phenomenological effects, mainly dealing with the effect at different pressures and beam powers as welding depth, as shown for example in [15–17]. Further process development shows the suitability for thick-walled components made of unalloyed steels and corrosion-resistant duplex steels [5,18]. Those components present reproducible high-quality joints on unalloyed steels (S355 to S690) up to 50 mm plate thickness on one side and up to 110 mm plate thickness with positional and counter-positional welding. They demonstrate an increasing welding depth of 200–300% by reducing the working pressure while the other parameters remain constant. Nowadays, this advantage of LaVa is already used in the series production of mobile powertrain components with welding depths of up to 25 mm on transmission construction [19]. The results of the stationary welds can be also transferred to a mobile, local vacuum chamber, which provides a reduced working pressure only in the immediate vicinity of the process zone. This mobile vacuum system (MoVac) can weld unalloyed steel plates with a thickness of 40 mm thick and joint gaps of up to 0.5 mm [6]. In the long term, a construction site mobile container unit is conceivable similar to the laser welded gas pipelines in [20]. Welding of pipelines or monopiles can be easily implemented thanks to the simple welding geometry and the existing knowledge of orbital welding. However, field studies still need to be carried out, firstly to demonstrate the feasibility, and secondly to investigate the influence of the entire process chain on the MoVac welding process. More complex components such as the butt joint of a T-beam would probably require a specially manufactured vacuum chamber, which still needs to be developed.

To increase the acceptance of the LaVa process, it is important to demonstrate the advantages by expanding the range of applications, such as the welding of galvanized thick sheets. Until now, galvanized sheets could only be welded with lasers to a limited extent, as the high intensity of the laser immediately vaporizes the zinc layer. In the automotive industry, the thin zinc sheets are often joined together in a lap joint, whereby the vaporizing material in the capillary behaves like a nozzle and leads to heavy spatter formation. In order to produce a solid welded joint with reduced spatter, a gap must be created in the design to allow the zinc to evaporate [21]. In the butt joint, galvanized sheets can only be joined with a uniformly defined cut edge and a suitable circular oscillation [22]. In this study, the cut edges produced with laser cutting present a lower strength compared to a shear cut, which is probably due to the oxidation of the cut edge. The variation of the gap due to the rough-cut edge, as well as the evaporating zinc, can be controlled by circular oscillation, as more material is melted on the one hand and pores from the solidified melt are melted again by the return movement of the laser. For fillet welds in an overlap configuration, tests show that a laser beam offset of approx. 0.2 mm to the weld produces a weld seam that is virtually pore-free. The high-speed images indicate that outgassing of the zinc through the capillary in the center must be made possible in order to avoid contamination [23]. Recent studies show that 1.2 mm thick galvanized steel sheets, which are used in the automotive industry, can be joined in butt joint configuration without additional wire and with a beam diameter of 600 µm [24]. Despite the high strength of the material of 490–590 MPa, the tensile specimens outside the weld seam travel with the strength of the base material. The associated bending tests also reach 180° without traveling. Identical results can also be seen in tests with a slightly thinner material of 1,0 mm an with a lower strength of 270–355 MPa [25]. In the area of thick-walled hot-dip galvanized sheets (>20 mm) that are used in steel constructions such as wind turbines, bridges, container ships or buildings, the authors are not aware of any investigations having been carried out and published.

The first self-conducted welding trials on hot-dip galvanized sheets with an electron beam welding process reveal the basic problem of the extreme evaporating zinc coating. The zinc layer evaporates at lower temperatures compared to iron [26] and therefore ejects the melting pool almost completely from the joining zone. As a result, the two parts are not joined together. Also, the large amount of evaporating zinc leads to significant fluctuations in the electron beam welding chamber, which causes vacuum instabilities during the welding process. A remedy is LaVa, which operates in a higher pressure range (0.1–100 mbar) compared to electron beam welding (<10^{-3} mbar) through which it is less vulnerable to vacuum fluctuations. In addition, as in electron beam welding, beam oscillation is possible, which can influence the capillary and the molten pool. Both together—pressure level and beam oscillation—offer the possibility to master the difficult welding processes of galvanized thick plates, which is investigated in this study.

3. Setup

Laser beam welding under vacuum was performed using the FOCUS LaVa 95 system, which allows a pressure regulation between 1–100 mbar. A TRUMPF TruDisk 16002 disk laser with a 200 µm fiber and a connected IPG D50 scanner optics produced a spot diameter of 400 µm at the focal point. The coaxially mounted camera STC-HD93DV from SENTECH made it possible to observe the welding process with a resolution of 1280 × 720 pixels and a frame rate of 60 FPS. An installed ring-shaped exhausting system removed the emissions from the beam path in addition to the OptiShield [27] that protects the coupling laser window, as shown in Figure 1. During the evacuation process, the ring-shaped suction unit was deactivated, and the vacuum chamber was pumped out via the main connection. When the target pressure was reached, shielding gas flowed into the chamber via the OptiShield, the main connection was closed, and further vacuum generation took place via the ring-shaped suction unit.

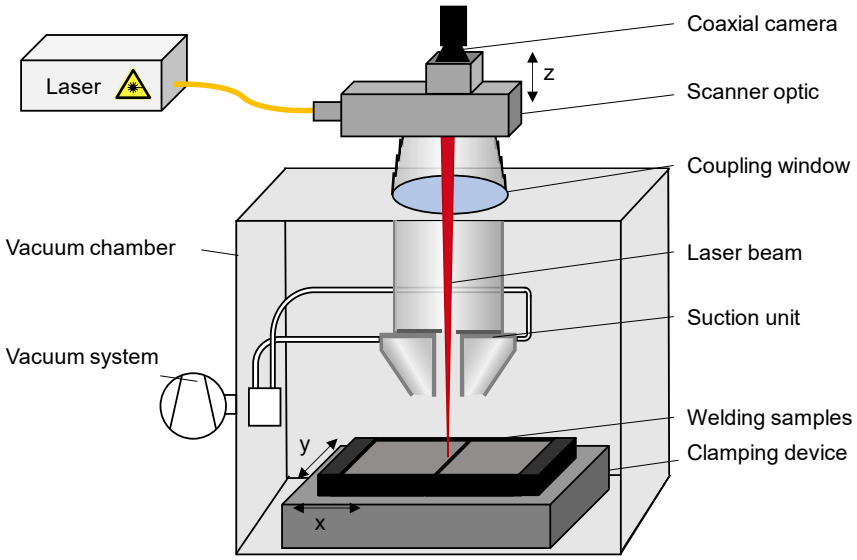

Figure 1. Vacuum system with welding setup.

The used constructional steel S355M with a thickness of 20 mm conducted a tensile strength between 470 and 630 MPa, according to DIN EN 10025-4 [28]. The chemical composition listed in Table 1 was analyzed with an optical emission spectroscopy (OES). The hot dip galvanizing of the material used an up to 98.5 wt% pure zinc coating, according to DIN EN ISO 1461 [29]. The zinc coating thicknesses on the top surface t_{top} of the samples varied between 200 and 400 µm depending on the batch.

Table 1. Chemical composition S355M measured with OES.

	C [wt%]	Si [wt%]	Mn [wt%]	P [wt%]	S [wt%]	Cr [wt%]	Nb [wt%]	Ti [wt%]	V [wt%]	Residual [wt%]
S355M	0.771	0.377	1.580	0.013	0.003	0.043	0.033	0.015	0.033	0.055

For the test, welding samples with dimensions of 20 × 120 × 150 mm were butt-jointed with different cut grades (saw cut, milled, flame cut). The zinc layer thickness in the joint gap was adjusted, specifically by making the cuts before or after the hot-dip galvanization. As a result, zinc layer thicknesses t_z in the joint gap varied between 0 and 800 µm. With a zinc layer thickness of t_z = 0 µm, the zinc layer was removed from both joining edges, while a zinc layer thickness of t_z = 800 µm referred to the sum of both joining edges in the butt joint configuration. The thickness of the zinc coating on the top of the sample and on the cut edge was measured and documented before each welding process.

About 155 welds were performed and analyzed in this study. The main outcomes are presented in this publication. Before the welds were performed with varying oscillation parameters, the welds were carried out with varying laser power P_L and welding speed vs. the non-galvanized samples at the constant working pressure p_{vac} to ensure sufficient welding penetration. After, the galvanized samples with zinc in the joining gap were used and the oscillation geometries (line, circle, infinity, triangle), the oscillation width A_{osc}, and the oscillation frequency f_{osc} were adjusted, as listed in Table 2. In the last iteration, the promising parameters were further used and welded with a variation of the focus position f_z.

Table 2. Investigated oscillation parameters.

	Line	Circle	Infinity	Triangle
A_{osc}[mm]	1–5	0.3–5	2–5.5	4
f_{osc}[Hz]	200	30–200	50–300	200

4. Results and Discussion

First, the welds were carried out on the ungalvanized sheet metal and the sheet metal that were only galvanized on the surface. The zinc in the joint gap was removed before welding. Later, the zinc layer in the joint gap was adjusted. Figure 2 presents the welding results of the ungalvanized samples for the identified parameter with a 0.3 mm circle oscillation geometry at a frequency of 80 Hz. The weld seams have almost parallel flanks and overlap sufficiently in the center of the sheet due to a welding depth of 11.0 mm. The 2.7 mm wide seam top scales were fine and uniform with a few isolated weld beads next to the weld seam, as shown in Figure 2a. The transfer of this parameter to only the surface galvanized sheets, where the zinc was removed from the joining edge (t_z = 0 µm), showed almost a similar welding result with a slightly increased welding depth to 12.6 mm. A burn-off of the t_{top} = 251 µm thick zinc layer on the surface extended approximately 5.6 mm to left and right of the weld seam: see Figure 2b. The weld top scales were finer and without isolated weld beads. One explanation for the finer fish scale could be related to the mill scale of the ungalvanized sheets being removed during the galvanizing process by several pretreatment steps before the specimen was admitted to the zinc tank. The slight increase in the penetration depth might be due to the tolerances of the gap in the butt joint.

Oscillation geometry	Circle
Laser power P_L [W]	5000
Welding speed v_s [mm/s]	7.67
Focus position f_z [mm]	0
Oscillation width A_{osc} [mm]	0.3
Oscillation frequency f_{OSC} [Hz]	80
Working pressure p_{vac} [mbar]	50
Zinc layer thickness t_z [µm]	0

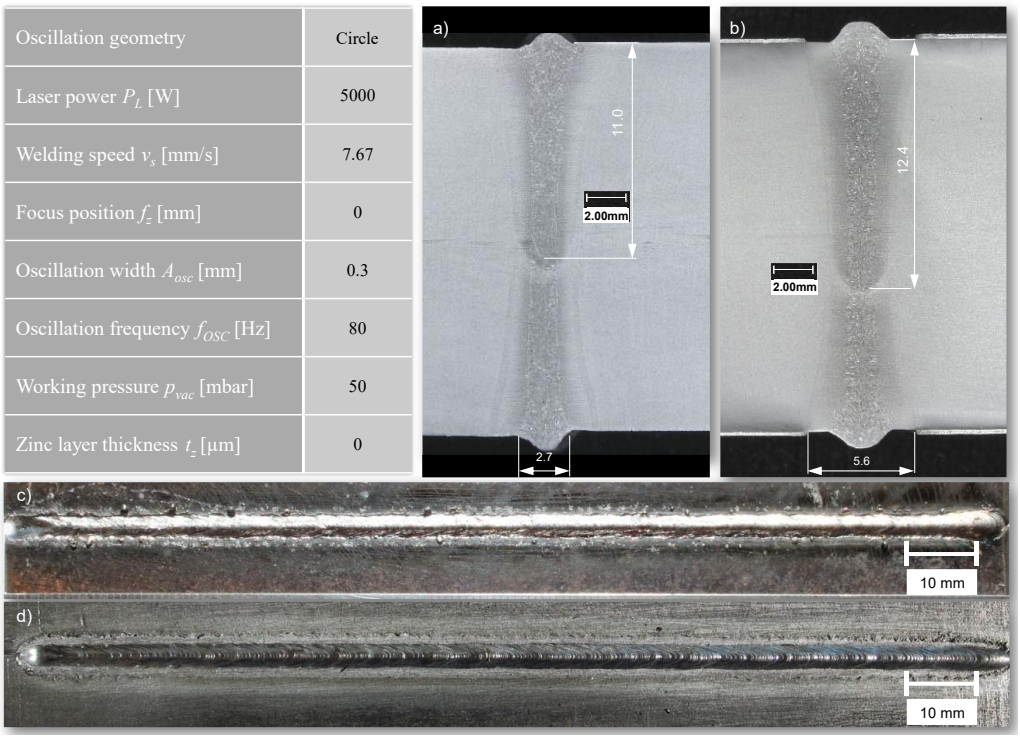

Figure 2. Welding parameters and comparison of (**a**) macro-section of non-galvanized and (**b**) surface galvanized sheet and removed zinc from the joining edge (t_z = 0 µm), (**c**) weld seam of non-galvanized and (**d**) surface galvanized sheet and removed zinc from the joining edge (t_z = 0 µm).

However, a direct transfer of the distance parameter to the samples with zinc in the joint gap was not successful. For the parameters with an oscillation width similar to the total zinc layer thickness t_z of the two welding samples in the joining gap (sum ~400–800 µm), all welding results presented an insufficient bonding, even for a 0.5 mm width circular geometry as shown in Figure 3. Regardless of the chosen oscillation geometry or frequency, the welding samples have partially melted zinc on the joining edge while the base material remained nearly unaffected. The laser beam formed a 400 µm diameter in focus and oscillated a 0.5 mm circle. This irradiated area covered mainly the zinc layer in the joint gap and only slightly the material on the workpiece surface, causing insufficient melted base material for the joint. As a result, a part of the laser energy vaporized the zinc while the rest passed through and hit the welding fixture.

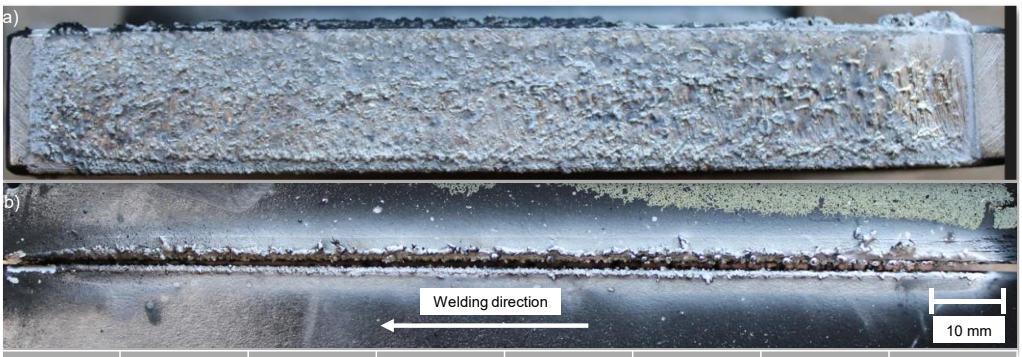

Oscillation geometry	P_L [W]	v_s [mm/s]	f_z [mm]	A_{osc} [mm]	f_{OSC} [Hz]	p_{vac} [mbar]	t_z [µm]
Circle	5833	5	0	0.5	30	50	458

Figure 3. Welding parameters and (**a**) surface of the galvanized joint edge and milled edge preparation showing no structural bond after welding and (**b**) top view.

As a result, increasing the oscillation width as an example of the infinity oscillation from 0.3 mm to 2 mm at a constant oscillation frequency of 200 Hz allowed the two zinc coated samples to bond together: see Figure 4. However, the melt pool drops through the gap were held back by the sheet metal of the fixture and connected the samples in the lower area only, as shown in Figure 4a. The edges of the samples in the upper area were only partly melted and remained parallel while significantly more laser power was applied to the lower area, which was visible through the heat-affected zone. A further increase in the oscillation width up to 4 mm at a nearly identical zinc layer thickness of 98 µm in the joining gap improved the seam drop: see Figure 4c. However, a thicker zinc layer of roughly 360 µm, while the oscillation widthstayed nearly the same, led to elongated pores and humping, as shown in Figure 4b. Inside the elongated pores, zinc deposited on the upper walls, which indicated that the evaporating zinc was not able to vanish through the capillary. Moreover, the zinc layer in the non-welded butt joint below the weld seam was also removed. One possible explanation for this effect is that the zinc at the welding depth itself can escape via the capillary, but not the zinc below the melt pool. This zinc layer also vaporizes when the temperature increases and the vapor pressure pushes the molten metal upwards, where it partially solidifies again on the walls. This theory would explain the welding result and the spatter-free welding process itself, but it can only be confirmed by X-ray analysis, as shown in [30]. The oscillation width of 5 mm at a constant laser power of 6300 W expanded the weld seam width, reduced the weld seam depth, and resulted in pore-free weld seams. The zinc layer below the weld, as marked in Figure 4d, remained unaffected. There were only marginal border notches on the weld seam. However, the welding process of this circular oscillation pattern was observed to be unstable with strong splashes that resulted in repeating investigations into the contamination of the coupling window and consequently to the termination of the welding process.

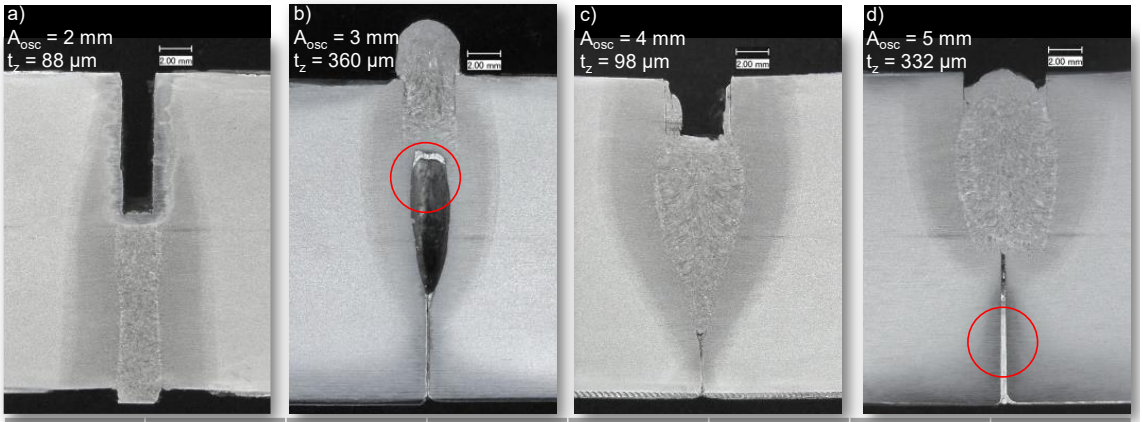

Oscillation geometry	P_L [W]	v_s [mm/s]	f_z [mm]	A_{osc} [mm]	f_{OSC} [Hz]	p_{vac} [mbar]	t_z [µm]
Infinity	6300	2	0	2–5	200	50	88–360

Figure 4. Welding parameters and influence of oscillation width on weld seam with remaining zinc circled in red for (**a**) flame cutting edge and t_z = 88 µm, (**b**) milled cutting edge and t_z = 360 µm, (**c**) flame cutting edge and t_z = 98 µm, (**d**) milled cutting edge and t_z = 332 µm.

Coaxial video recordings were made to identify the cause of the heavy spatter formation and consequently to improve the process. As is known, the metal flow and fluid dynamic strongly depend on the oscillation parameters [31]. Therefore, the beam oscillation geometry was adjusted to improve the evaporation of zinc while reducing the spatter formation. A visual observation with a coaxial camera made it possible to qualitatively evaluate the process behavior and welding result. Figure 5a shows the recording of the circular oscillation. The molten pool forms according to the oscillation figure. The video recordings show qualitatively that the spatter formation took place at the front and rear of the circular oscillation, at the transition of the joining gap and in the middle of the melt

pool, as schematically shown in Figure 5b. Identical behavior was also observed for the triangular oscillation, which is why this figure was not investigated any further. Based on the video recordings and the findings from the literature listed in the previous article, it was concluded that it is not advantageous for a melt pool to be generated in the middle of the joint. On the contrary, the zinc must evaporate via the capillary, as shown in [21].

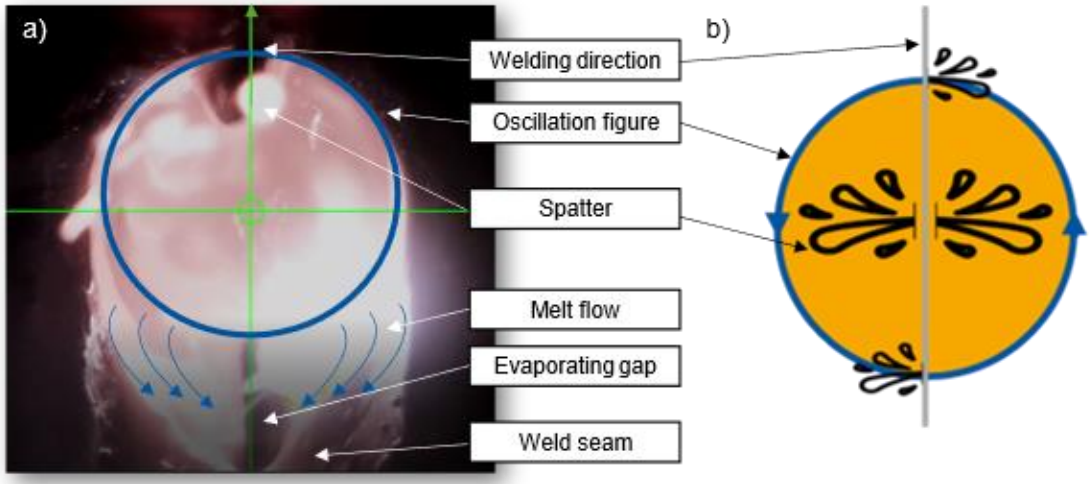

Figure 5. (**a**) Snapshot of camera recording for 5 mm circular oscillation; (**b**) schematic view of the observed spatters.

Figure 6a shows a camera view with the line oscillation, where the molten pool is shaped like a downward-rotated triangle. Using the chosen line oscillation, the laser beam oscillates perpendicular to the welding direction. The liquid metal from both sheets flows backwards and merges behind the welding gap, which allows the zinc to evaporate through the gap. The process was smooth with little to no spatters compared to the circular oscillation. The images show only isolated spatter, which can be detected later on or next to the weld seam, as can be seen in Figure 7. However, the recordings are limited due to the interfering metal vapor, low resolution, and frame rate of the camera, which need to be considered. Nevertheless, the videos give a qualitative insight.

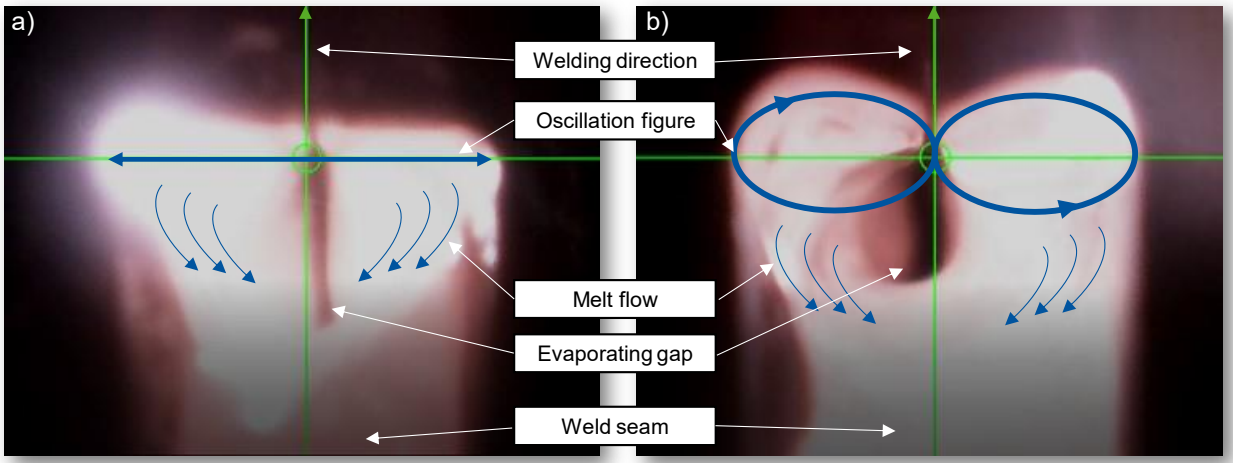

Figure 6. Snapshot of camera recording for 5 mm (**a**) line and (**b**) infinity oscillation.

Oscillation geometry	P_L [W]	v_s [mm/s]	f_z [mm]	A_{osc} [mm]	f_{OSC} [Hz]	p_{vac} [mbar]	t_z [µm]
Line	6300	2	−7.5	5	200	50	339

Figure 7. Welding parameters and (**a**) weld seam with linear oscillation; (**b**) macro-section of the weld seam with milled edge preparation.

However, the line oscillation geometry produced pores and seam bulging even at a large oscillation width of 5 mm, as shown in Figure 7. Similar to the infinity oscillation, as shown in Figure 4b, in the line oscillation the evaporating zinc below the melt pool was not able to vanish through the welding gap and pushed the liquid metal up, resulting in a long-drawn pore.

The oscillation of the laser beam in an infinity geometry along the welding direction is shown in Figure 6b. It shows a slightly bigger round gap between the two melt pools on each sheet. Out of this round gap, the zinc evaporates while the melt pool flows around. The opening of the round gap is almost constant over the whole welding process and produces almost no spatters. The welding result of the infinity oscillation geometry shows uniform seam scaling with a seam undercut, see Figure 8a. The zinc on the surface evaporates in an area roughly 15.3 mm next to the weld seam due to the high process temperature. This area and the weld seam must be subsequently protected against corrosion in the future. It is not possible to avoid the seam undercut as material is missing in the joint gap due to the evaporating zinc and no filler material is used. The macro section of this oscillation pattern, as shown in Figure 8b–e, indicates no pores and a rising seam undercut with an increasing zinc layer thickness. The oscillation parameters are identical while the zinc layer thickness t_z rises from 0 µm up to 664 µm in the joining gap.

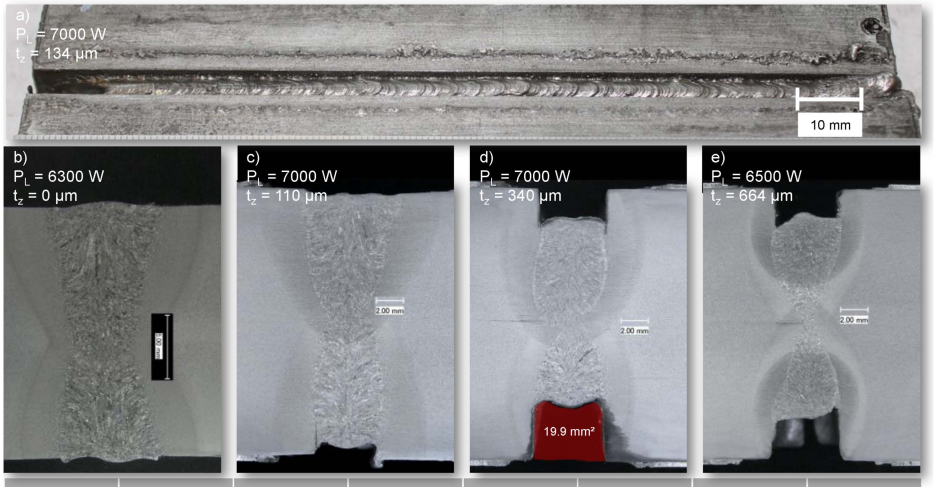

Oscillation geometry	P_L [W]	v_s [mm/s]	f_z [mm]	A_{osc} [mm]	f_{OSC} [Hz]	p_{vac} [mbar]	t_z [µm]
Infinity	6300-7000	3.5	-7.5	5	200	50	0-664

Figure 8. Welding parameters and weld seams with infinity oscillation and macro-sections of the weld at various zinc layer thicknesses in the joining edge (**a**) weld seam (**b**) zinc removed with saw cut (**c**) flame cutting (**d**,**e**) milled edge preparation.

Assuming a total zinc layer thickness of 400 µm in the joining gap, the missing cross-sectional area calculates 8 mm^2 for a sheet thickness of 20 mm. With a 600 µm total zinc coating thickness, this results in a lack of the 12 mm^2 cross section area that needs to be filled. In addition, a part of the base material evaporates as well. Depending on how well the material can flow from the base material, the missing area is bridged. For example, macro-section images in Figure 8d measure an area of the missing material of up to 19.9 mm^2 for a zinc layer thickness of 340 µm. Using the identical galvanizing parameters, the zinc layer thickness in the joint gap is mainly determined by the prepared cutting edge. While the zinc layer thickness is the same for cold cutting processes such as water jet, milling, and sawing, that of flame cutting deviates significantly. The burn-off of the alloying elements on the cut edge inhibits the galvanizing process [32], resulting in a zinc coating thicknesses of up to only 100 µm. In addition, however, there is an arithmetic mean roughness value of R_a = 2.12 µm, which is only R_a = 0.61 µm in the case of milling. A comparison of the influence of the arithmetic mean roughness value or waviness on the welding process cannot be made due to the highly differing zinc coating thicknesses.

The project idea is based on the hypothesis that the zinc in the joint gap can serve as an alloy of the weld and thus influence the mechanical–technological properties of the weld seam. However, the hardness measurements according to Vickers and energy dispersive X-Ray spectroscopy (EDX) analyses do not show any indication of this, as shown in Figure 9.

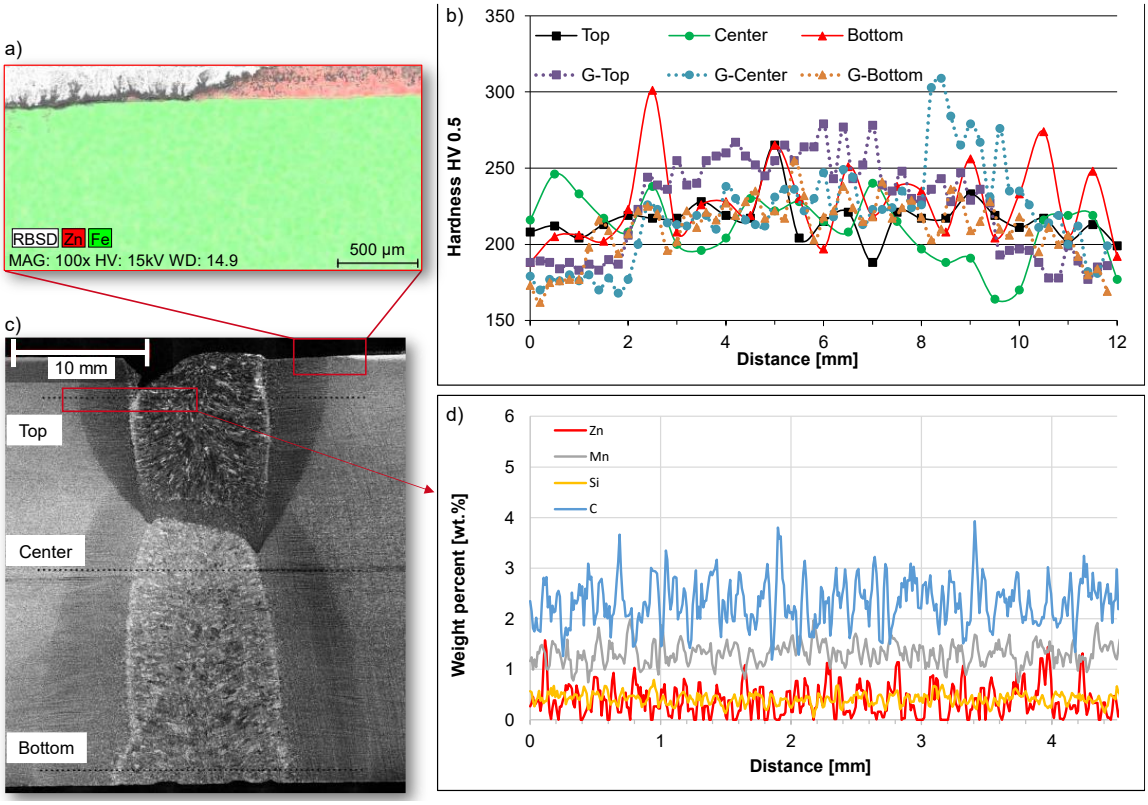

Figure 9. Vickers hardness and EDX measure of weld seam to analyze zinc in weld seam. (**a**) element mapping (**b**) comparison of weld seam hardness (**c**) macro section of weld seam (**d**) element line scan for base material and weld seam.

Figure 9b presents the hardness test of the two welding samples, and both were performed with identical laser parameters. The straight lines indicate the hardness of the welding sample without zinc in the joining gap, measured on the top, center, and bottom of the weld. The dotted lines depict the hardness test for the galvanized samples, shown in Figure 9c, having a 200 µm zinc layer in the joining gap. There is a slight increase in

hardness values in the weld area but no significant trend difference between galvanized and non-galvanized specimen. The measured values are in a similar range. For example, the hardness measurement of the ungalvanized sample shows a maximum value of 301 HV, but this is to be declared as an outlier, similar to the maximum hardness measurement of the galvanized sample of 309 HV. Both values are harmless for real applications since the majority of the measured values are in the range of the base material. The EDX line measurement in Figure 9d indicates that no zinc binds were in the weld. The fluctuations around the mean value of 0.39 wt.% are due to the measurement inaccuracies and surface deposition caused by the grinding process of the specimen. There is also no diffusion of the upper zinc layer with the base material due to the high process temperatures, as confirmed in Figure 9a. The zinc layer essentially evaporates. The area of the surface measurement highlighted as white shows the material of the embedding of the specimen. Thus, no influence of the zinc on the mechanical–technological properties of the weld metal is measurable. Tensile tests were also carried out occasionally to check the influence of the zinc on the weld seam. However, these behaved as well known in [33], that the fracture propagates in the base material and thus assumes its strength values of approximately 570 MPa. It is therefore not possible to draw any conclusions about the influence of the zinc on the weld seam, and this underlines the EDX results that there is no zinc in the weld metal.

5. Conclusions

The aim of this work was to investigate the weldability of hot-dip galvanized thick plates by laser beam welding under vacuum, since this process chain has great economic potential in steel construction. For this purpose, welding tests were successfully carried out on 20 mm thick S355M steel sheets with different edge preparations. In the case of sheets with a galvanized joining edge, joining has proved to be difficult because the zinc evaporates from the gap under the action of the laser and entrains the molten metal. However, this effect could be reduced by using a beam oscillation width of 5 mm and an infinity oscillation geometry at an oscillation frequency of 200 Hz. The infinity oscillation geometry reduces the spatter formation, lowers the seam drop, and prevents pores. In contrast, the circle, triangle, and line oscillation geometries did not show sufficient weld quality. This can be attributed to the changing melt pool flows. In addition, it could be shown that the seam drop is reduced by the infinity, but not completely suppressed due to the lack of material in the joining gap once the zinc has evaporated. The reduced zinc layer in the joining gap due to the flame cut could be used to set different zinc layer thicknesses and consequently investigate its influence on the welding process. This varied between 70 and 120 µm. No difference was found between the cold cutting processes of sawing and milling. The zinc layer thickness in the joint gap with these processes was between 300 and 670 µm. With an increasing zinc layer thickness on the joining edge, the negative influence on the weld quality increases further.

Author Contributions: Conceptualization and validation, C.F.; investigation, C.F. and O.S.; writing—original draft preparation, O.S.; writing—review and editing, C.F. and R.K.; visualization, C.F.; supervision, S.O.; project administration, M.F. and U.R. All authors have read and agreed to the published version of the manuscript.

Funding: The research project IGF 21487 N/P1416 "Erweiterung der Einsatzgebiete von feuerverzinkten Stahlbauteilen in Kombination mit Strahlschweißverfahren" from the Research Association for steel Application (FOSTA), Düsseldorf, is supported by the Federal Ministry of Economic Affairs and Climate Action the German Federation of Industrial Research Associations (AiF) as part of the program for promoting industrial cooperative research (IGF) on the basis of a decision by the German Bundestag. The project is carried out at the Welding and Joining Institute RWTH Aachen and Institute of Steel Constructions RWTH Aachen.

Data Availability Statement: The data that support the findings of this study are available from the corresponding author under the following link (http://hdl.handle.net/21.11102/a8a687df-478c-4614-bd3d-84073f3c6aa7 accessed on 27 December 2023) and upon reasonable request.

Conflicts of Interest: The authors declare no conflicts of interest. The funders had no role in the design of the study; in the collection, analyses, or interpretation of data; in the writing of the manuscript; or in the decision to publish the results.

References

1. Börner, C.; Krüssel, T.; Dilger, K. Process characteristics of laser beam welding at reduced ambient pressure. In *High-Power Laser Materials Processing: Lasers, Beam Delivery, Diagnostics, and Applications II*; Dorsch, F., Ed.; SPIE: Bellingham, DC, USA, 2013; pp. 1–13.
2. Ungermann, D.; Holtkamp, S.; Rademacher, D.; Hechler, O.; Pinger, T. Anwendung der Feuerverzinkung im Brückenbau. In *STAHLBAU KALENDER 2017: Dauerhaftigkeit Ingenieurtragwerke*; Kuhlmann, U., Ed.; Wiley: Hoboken, NJ, USA, 2017; pp. 767–812.
3. Pinger, T. Zur Vermeidung der Rissbildung an Stahlkonstruktionen beim Feuerverzinken Unter Besonderer Berücksichtigung der Flüssigmetallinduzierten Spannungsrisskorrosion. Ph.D. Thesis, Shaker, Aachen, Germany, 2009.
4. BASt—Bundesanstalt für Straßenwesen. *Zusätzliche Technische Vertragsbedingungen und Richtlinien für Ingenieurbauten (ZTV-ING)*; Bundesministerium für Digitales und Verkehr: Bonn, Germany, 2022.
5. Jakobs, S. Laserstrahlschweißen im Vakuum: Erweiterung der Prozessgrenzen für Dickwandige Bleche. Ph.D. Thesis, Shaker Verlag, Herzogenrath, Germany, 2015.
6. Gerhards, B.; Schleser, M.; Otten, C. Laser beam welding with mobile vacuum: MoVac. In *High-Power Laser Materials Processing: Applications, Diagnostics, and Systems X*; Kaierle, S., Heinemann, S.W., Eds.; SPIE: Bellingham, DC, USA, 2021; p. 6.
7. Thiele, M.; Schütz, A.; Schulz, W.D. *Struktur und Eigenschaften von Zinküberzügen Nach DIN EN ISO 1461 Aus Legierten Zinkschmelzen in Abhängigkeit vom Si-Gehalt des Stahlwerkstoffes, den Verzinkungsbedingungen und den Abkühlbedingungen*; AiF: Dresden, Germany, 2008.
8. Stahl-Informations-Zentrum. *Merkblatt 400-Korrosionsverhalten von Feuerverzinktem Stahl*, 6th ed.; Stahl-Zentrum: Düsseldorf, Germany, 2001.
9. Schulz, W.-D.; Thiele, M. *Feuerverzinken von Stückgut*, 2nd ed.; Leuze-Verlag: Bad Saulgau, Germany, 2012.
10. *DIN EN ISO 14713:(14713)*; Leitfäden und Empfehlungen zum Schutz von Eisen- und Stahlkonstruktionen vor Korrosion. Deutsches Institut für Normung e. V.: Berlin, Germany, 2020.
11. Lappalainen, E.; Unt, A.; Sokolov, M.; Vänskä, M.; Salminen, A. Laser welding with high power Lasers: The effect of joint configuration. In Proceedings of the 14th NOLAMP Conference: The 14th Nordic Laser Materials Processing Conference, Gothenburg, Sweden, 26–28 August 2013; Luleå University of Technology, Department of Engineering Sciences and Mathematics, Division of Product and Production Development: Luleå, Sweden, 2013; pp. 133–144.
12. Sokolov, M.; Salminen, A.; Katayama, S.; Kawahito, Y. Reduced pressure laser welding of thick section structural steel. *J. Mater. Process. Technol.* **2015**, *219*, 278–285. [CrossRef]
13. Feldmann, M.; Pinger, T.; Schäfer, D.; Pope, R.; Smith, W.; Sedlacek, G. *Hot-Dip-Zinc-Coating of Prefabricated Structural Steel Components*; Italien: Aachen, Germany, 2010.
14. Arata, Y.; Abe, N.; Oda, T.; Tsujii, N. Fundamental phenomena during vacuum laser welding. *ICALEO Proc.* **1984**, *44*, 1–7. [CrossRef]
15. Abe, Y.; Mizutani, M.; Kawahito, Y.; Katayama, S. Deep penetration welding with high power laser under vacuum. *Int. Congr. Appl. Lasers Electro-Opt.* **2010**, *2010*, 648–653. [CrossRef]
16. Katayama, S.; Kobayashi, Y.; Mizutani, M.; Matsunawa, A. Effect of vacuum on penetration and defects in laser welding. *J. Laser Appl.* **2001**, *13*, 187–192. [CrossRef]
17. Reisgen, U.; Olschok, S.; Jakobs, S. Laser beam welding under vacuum in comparison to electron beam welding. *Weld. Cut.* **2010**, *9*, 224–230.
18. Turner, C. Erweiterung der Anwendungsfelder des Laserstrahlschweißens im Vakuum auf Duplex-Stahl und Kupfer. Ph.D. Thesis, Rheinisch-Westfälische Technische Hochschule Aachen, Aachen, Germany, 2019.
19. Jiang, M.; Tao, W.; Chen, Y. Laser Welding under Vacuum: A Review. *Appl. Sci.* **2017**, *7*, 909. [CrossRef]
20. Keitel, S.; Kocks, H.-J.; Raschke, A. Einsatz des Laserstrahlschweißens beim Bau Einer Gaspipeline. *DVS Berichte* **2018**, *344*, 161–166.
21. Hao, Y.; Wang, H.-P.; Sun, Y.; Li, L.; Wu, Y.; Lu, F. The evaporation behavior of zinc and its effect on spattering in laser overlap welding of galvanized steels. *J. Mater. Process. Technol.* **2022**, *306*, 117625. [CrossRef]
22. Zhang, Z.; Zhao, Y.; Wu, S.; Lu, H. Optimization of butt welding of zinc-coated thin sheets with oscillating fiber laser beams: Weld formation, microstructure, and mechanical properties. *Weld World* **2021**, *65*, 1711–1723. [CrossRef]
23. Roos, C.; Schmidt, M. Remote Laser Welding of Zinc Coated Steel Sheets in an Edge Lap Configuration with Zero Gap. *Phys. Procedia* **2014**, *56*, 535–544. [CrossRef]
24. Górka, J.; Suder, W.; Kciuk, M.; Stano, S. Assessment of the Laser Beam Welding of Galvanized Car Body Steel with an Additional Organic Protective Layer. *Materials* **2023**, *16*, 670. [CrossRef] [PubMed]

25. Rezeznikiewicz, A.; Górka, J.; Przybyla, M.; Kciuk, M. Assessment of properties and corrosion resistence of galvanized steel welded with laser beam. *Int. J. Mod. Manuf. Technol.* **2023**, *XV*, 155–166.
26. Honig, R.E.; Krammer, D.A. Vapor data pressure for the solid and the liquid elements. *RCA Rev.* **1969**, *30*, 285–305.
27. Jakobs, S.; Reisgen, U.; Olschok, S.; Klein, S. *Unterdruckkammer Mit Einem Schutzgehäuse (DE 10 2014 103 635 A1)*; Deutsches Patent- und Markenamt: München, Germany, 2015.
28. *DIN EN 10025-4*; Warmgewalzte Erzeugnisse aus Baustählen-Teil 4. Deutsches Institut für Normung e. V.: Berlin, Germany, 2023.
29. *DIN EN ISO 1461*; Durch Feuerverzinken Auf Stahl Aufgebrachte Zinküberzüge (Stückverzinken). Deutsches Institut für Normung e. V.: Berlin, Germany, 2022.
30. Wagner, J.; Hagenlocher, C.; Hummel, M.; Olowinsky, A.; Weber, R.; Graf, T. Synchrotron X-ray Analysis of the Influence of the Magnesium Content on the Absorptance during Full-Penetration Laser Welding of Aluminum. *Metals* **2021**, *11*, 797. [CrossRef]
31. Zhang, C.; Li, X.; Gao, M. Effects of circular oscillating beam on heat transfer and melt flow of laser melting pool. *J. Mater. Res. Technol.* **2020**, *9*, 9271–9282. [CrossRef]
32. *DIN EN ISO 14713-2*; Zinküberzüge–Leitfäden und Empfehlungen zum Schutz von Eisen-und Stahlkonstruktionen vor Korrosion-Teil 2. Deutsches Institut für Normung e. V.: Berlin, Germany, 2022.
33. Hollmann, P.; Drechsel, J.; Zenker, R.; Löschner, U.; Biermann, H. Comparative Studies on Electron Beam and Laser Beam Welding of QT-Steel and Structural Steel. *HTM J. Heat Treat. Mater.* **2019**, *74*, 331–341. [CrossRef]